Nanoscale

PAPER

View Article Online
View Journal | View Issue

Cite this: *Nanoscale*, 2015, **7**, 7415

Arginine-assisted immobilization of silver nanoparticles on ZnO nanorods: an enhanced and reusable antibacterial substrate without human cell cytotoxicity†

Shekhar Agnihotri,[a] Geetika Bajaj,[a] Suparna Mukherji[a,b] and Soumyo Mukherji*[a,c,d]

Received 21st November 2014,
Accepted 15th February 2015

DOI: 10.1039/c4nr06913g

www.rsc.org/nanoscale

Silver-based hybrid nanomaterials are gaining interest as potential alternatives for conventional antimicrobial agents. Herein, we present a simple, facile and eco-friendly approach for the deposition of silver nanoparticles (AgNPs) on ZnO nanorods, which act as a nanoreactor for *in situ* synthesis and as an immobilizing template in the presence of arginine. The presence of arginine enhanced the stability of ZnO deposition on the glass substrate by hindering the dissolution of zinc under alkaline conditions. Various Ag/ZnO hybrid nanorod (HNR) samples were screened to obtain a high amount of silver immobilization on the ZnO substrate. Ag/ZnO HNRs displayed potent antibacterial ability and could achieve 100% kill for both *Escherichia coli* and *Bacillus subtilis* strains under various test conditions. The hybrid material mediated its dual mode of antibacterial action through direct contact-killing and release of silver ions/nanoparticles and showed superior bactericidal performance compared to pure ZnO nanorods and colloidal AgNPs. No significant decline in antibacterial efficacy was observed even after the same substrate was repeatedly reused multiple times. Interestingly, the amount of Ag and Zn release was much below their maximal limit in drinking water, thus preventing potential health hazards. Immobilized AgNPs showed no cytotoxic effects on the human hepatocarcinoma cell line (HepG2). Moreover, treating cells with the antibacterial substrate for 24 hours did not lead to significant generation of reactive oxygen species (ROS). The good biocompatibility and bactericidal efficacy would thus make it feasible to utilize this immobilization strategy for preparing new-generation antibacterial coatings.

1. Introduction

Considering the potential health risks associated with the emergence of multidrug-resistant bacteria and greater incidences of cross contamination, the development of new and effective bactericidal agents is of utmost concern.[1,2] The interest in nano-silver based antimicrobial materials is increasing worldwide and is corroborated by the large number of research articles published in this area during the past decade.[3,4] Compared to colloidal AgNPs, immobilized silver nanoparticles are physico-chemically more stable as they are less prone to aggregation and oxidation when exposed to the aqueous medium.[5–7] Thus, they retain long-term antibacterial efficacy. Moreover, immobilization of silver nanoparticles on a support matrix facilitates ease of handling and reusability and minimizes toxic effects associated with their inevitable discharge into the aqueous ecosystem.[7,8] Reportedly, silver nanoparticles can be incorporated on hybrid materials either by impregnating AgNPs within porous matrices[9] or by anchoring them on surface-functionalized solid supports.[10,11] Silver nanoparticles immobilized on various inorganic and organic substrates such as SiO_2, Fe_2O_3, zinc oxide, and graphene have demonstrated an enhanced antibacterial performance over long term use.[7,12–14]

Other than metallic silver, zinc oxide (ZnO) has also been widely reported to inhibit and inactivate microbial growth at the nanoscale. Being relatively cheaper, non-toxic, and biocompatible, ZnO is an important ingredient for various cosmetic products and antibacterial lotions and is commonly used as a drug carrier and filler in dental materials.[15,16] The use of

[a]*Centre for Research in Nanotechnology and Science, Indian Institute of Technology-Bombay, Powai, Mumbai 400076, India*
[b]*Centre for Environmental Science and Engineering, Indian Institute of Technology-Bombay, Powai, Mumbai 400076, India*
[c]*Department of Biosciences and Bioengineering, Indian Institute of Technology-Bombay, Powai, Mumbai 400076, India*
[d]*Centre of Excellence in Nanoelectronics, Indian Institute of Technology-Bombay, Powai, Mumbai 400076, India. E-mail: mukherji@iitb.ac.in; Fax: +91-22-2572 3480; Tel: +91-22-2576-7767*

†Electronic supplementary information (ESI) available: Synthesis of ZnO nanorods, instrumentation details, contact killing of Ag/ZnO. See DOI: 10.1039/c4nr06913g

Ag/ZnO based hybrid nanostructures has recently gained much interest not only because of their ease of fabrication through various routes, but also due to their comparatively higher photocatalytic efficiency and synergistic antibacterial activity than their individual forms.[16,17] To date, a variety of methods have been explored for the incorporation of Ag on to ZnO support material through doping, ultrasonication, the solvothermal method, pulsed layer deposition, irradiation assisted anchoring or *in situ* synthesis of AgNPs.[13,18–21] From the point of view of immobilization, silver nanoparticles can readily self-assemble on ZnO templates as they provide both anchoring sites for the metal ions to bind and nucleation sites for their subsequent growth. However, in the absence of any binder/linker, it is extremely difficult to control the dispersivity, stability and loading of silver nanoparticles over ZnO surfaces.[20] As a result, AgNPs may get easily desorbed from the ZnO surface when exposed to harsh experimental conditions, thereby limiting its long term usage. Therefore, it is highly desirable to develop an effective approach for localized deposition of AgNPs on the surface-functionalized ZnO nanostructures without compromising their bactericidal efficacy.

Amino acids possess high affinity towards metals and metal oxides. Among all the amino acids, arginine has the highest affinity towards silver ions,[22] which may bind at various electron rich sites, *i.e.*, nitrogen atoms of α-amino groups as well as guanidino side chains, in addition to carboxyl moieties at the C-terminus, forming stable silver–arginine complexes. On the other hand, arginine is also known to involve in surface modification of zinc oxide as a ZnO-binding polypeptide.[23,24] However, to the best of our knowledge, arginine-assisted immobilization of silver nanoparticles on ZnO nanorods under ambient conditions has not been attempted to date.

Although considerable success has been achieved in enhancing the bactericidal action of Ag/ZnO nanocomposites, surprisingly some important aspects are yet to be explored. There are only a limited number of reports in which Ag/ZnO nanocomposites have been evaluated on the basis of their silver/zinc release in aqueous medium, reusability, durability, long-term antimicrobial efficacy and cytotoxic effects on human or mammalian cells. Li *et al.*[13] recently demonstrated the long-term antimicrobial activity and reusability of Ag/ZnO nanomaterial for wound dressing applications. Similarly, Motshekga *et al.*[20] have reported better disinfection performance of the Ag/ZnO nanocomposite supported on Bentonite clay, where the leaching of silver from the nanocomposite was found to be within the acceptable limits specified for potable water. However, in order to establish the biocidal potential of Ag/ZnO hybrid nanomaterial for diverse applications, all the aforementioned aspects need to be discussed in one study.

In this study, we describe a facile and greener approach for dense immobilization of silver nanoparticles on ZnO nanorods using arginine as the linker molecule for potential antibacterial purposes. The reaction conditions were optimized to achieve maximum immobilization of AgNPs over ZnO nanorods to maximize the bactericidal potential. Antibacterial tests for Ag/ZnO hybrid material against both Gram-positive and Gram-negative bacterial strains were performed at two initial cell concentrations (10^3 CFU ml^{-1} and 10^5 CFU ml^{-1}) in a 100 ml batch reactor. The bactericidal efficacy and the corresponding silver release profile of the same AgNP/ZnO substrate were also evaluated over multiple wash and reuse cycles in order to determine its potential for practical applications. Cytotoxicity analysis of Ag/ZnO nanomaterial was performed using the human HepG2 cell line as an *in vitro* model to test its biocompatibility and applicability as antibacterial coatings for promising biomedical applications.

2. Experimental details

Materials required

Zinc acetate dihydrate ($Zn(CH_3COO)_2{\cdot}2H_2O$, ≥98% pure), zinc nitrate hexahydrate ($Zn(NO_3)_2{\cdot}6H_2O$, ≥98% pure), and lithium hydroxide monohydrate ($LiOH{\cdot}H_2O$, ≥98% pure) were received from Sigma-Aldrich (USA). Hexamethylenetetramine (HMTA, $C_6H_{12}N_4$, ≥99% pure), silver nitrate ($AgNO_3$, >99.9% pure), L-arginine ($C_6H_{14}N_4O_2$, ≥99% pure) and ascorbic acid ($C_6H_8O_6$, ≥99% pure) were purchased from Merck (India). *Escherichia coli* MTCC 443 (ATCC 25922) and *Bacillus subtilis* MTCC 441 (ATCC 6633) were used as test strains for conducting antibacterial experiments. They were originally procured from the Institute of Microbial Technology (Chandigarh, India). Nutrient medium (Himedia Pvt Ltd, Mumbai) was used for growing bacteria in liquid broth culture as well as preparing solid medium for plate culture studies by adding 2% bacteriological agar (Himedia Lab. Ltd, Mumbai).

For cytotoxicity tests, human hepatocarcinoma cell lines (HepG2) were obtained from the National Centre for Cell Sciences, Pune, India. Phosphate buffered saline (PBS) was purchased from Himedia Pvt Ltd, Mumbai, India. Dulbecco's modified Eagle's medium (DMEM), fetal bovine serum, 10^4 U ml^{-1} penicillin, 10 mg ml^{-1} streptomycin, and 25 μg ml^{-1} Amphotericin-B were procured from Gibco (USA). 3-(4,5-Dimethyl-thiazol-2-yl)-2,5-diphenyl tetrazolium bromide (MTT) dye, Triton X-100, tertiary butyl hydroperoxide (t-BH) and 2,7-dichlorofluorescein diacetate (DCFDA) dye were purchased from Sigma-Aldrich (USA). All chemicals were used as received without further purification. Ultrapure water (resistivity 18.2 MΩ cm) was used for all synthesis reactions and bacteriological experiments.

Synthesis of AgNP–ZnO hybrid nanorods

ZnO nanorods were synthesized through a two-step alcothermal seeding and hydrothermal growth process (refer to section S1† in ESI). Aqueous solution of arginine–silver complexes was prepared as reported earlier.[25] Five sets of silver–arginine complexes (aq.) were synthesized having the molar concentrations of $AgNO_3$ of 5, 10, 20, 25, and 75 mM such that the molar ratio of silver : arginine was kept constant at 5 : 2. ZnO NRs grown on glass surfaces (2 × 2.3 cm^2) were immersed in a freshly prepared silver–arginine mixture of various concentrations (5 to 75 mM) for 12 hours to facilitate interaction between the ZnO

NRs with the silver–arginine complex. Subsequently, the substrates were removed, washed with DI water and sonicated for 10 seconds to remove loosely bound silver. This was followed by *in situ* reduction of silver ions using a non-toxic reducing agent, *i.e.*, ascorbic acid. The silver loaded ZnO glass substrates were dipped in an ascorbic acid solution (100 mM, 50 ml) for 30 minutes resulting in *in situ* reduction followed by immobilization of AgNPs over the surface of ZnO NRs. Samples were thoroughly rinsed and sonicated as mentioned in the earlier step. To designate various AgNP–ZnO hybrid nanorod (HNR) samples, substrates incubated in a silver–arginine solution mixture containing 5 mM, 10 mM, 20 mM, 25 mM, and 75 mM $AgNO_3$ are referred to as Ag/ZnO-5, Ag/ZnO-10, Ag/ZnO-20, Ag/ZnO-25, and Ag/ZnO-75 HNRs, respectively, in the following studies. The mass loading of silver in the immobilized substrates was quantified using inductively coupled plasma-atomic emission spectroscopy (ICP-AES, refer to section S2† in ESI). Finally, the silver content on Ag/ZnO HNRs (μg cm^{-2}) was calculated by normalizing the amount of silver extracted from the substrate, with the total surface area of Ag/ZnO HNRs deposited on the glass substrate.

Antibacterial studies

Strain specific antibacterial activity of Ag–ZnO HNRs was determined against Gram-negative *Escherichia coli* MTCC 443 and Gram-positive *Bacillus subtilis* MTCC 441 strains. Two sets of independent antibacterial tests were performed using deionized water (DI) and a chlorine-free phosphate buffer as the test solution, as described in our earlier study.[7] The Ag–ZnO glass substrate (2 × 2.3 cm^2) was suspended centrally in a batch reactor (100 ml) having either 10^3 or 10^5 CFU ml^{-1} initial bacterial concentration, and sampling was performed over a period of 1–2 hours. Size-controlled, monodispersed colloidal AgNPs of average size 10 ± 2 nm, synthesized following the protocol discussed in our recent study,[26] were used in antibacterial studies for comparing their bactericidal activity with immobilized Ag/ZnO HNRs. The total mass of silver in colloidal AgNPs (in the 100 ml batch reactor) was kept at 6.0 × 10^{-2} mg, which was similar to that in the immobilized system (*i.e.*, Ag/ZnO HNRs). Silver nanoparticles immobilized on a flat amine functionalized silica substrate[7] (AgNP-silica) was also considered in order to compare the two 'immobilized systems', *i.e.*, AgNP-silica and Ag/ZnO HNRs for their antibacterial action under similar test conditions. For each experiment, the bacterial aliquots (100 μl) were homogeneously plated on agar plates, and incubated at 37 °C to count the viable bacterial colonies after 24 hours. All studies were done in duplicate. The zone of inhibition (ZoI) assay was done to compare the bactericidal potential of AgNP/ZnO HNR substrates with that of pure ZnO NRs. For this, the substrates were individually placed on an agar plate having uniform bacterial suspension (*E. coli* MTCC 443, 10^5–10^6 CFU ml^{-1}) and the culture plates were incubated at 37 °C for 24 hours. Both substrates (*i.e.*, AgNP/ZnO HNRs and pure ZnO NRs) were screened on the basis of the zone of inhibition (ZoI) using photographic images of the culture plates. For determining the contact-killing biocidal action of the material, Ag/ZnO-20 HNRs deposited on the glass substrate (2 × 2.3 cm^2) were placed in direct contact with solid agar having a uniform bacterial lawn (*E. coli*, 10^5–10^6 CFU ml^{-1}) for one hour to express its antibacterial effects. After one hour, the substrate was carefully removed and the culture plate was incubated for 24 hours at 37 °C.

To demonstrate the reuse potential of the hybrid antibacterial material, a single AgNP–ZnO HNR substrate was utilized several times for disinfection experiments. Concurrently, the silver and/or zinc release profile was also evaluated. The same antibacterial substrate (2 × 2.3 cm^2) was used 11 times alternately, such that each n^{th} and $n + 1^{th}$ study denotes a disinfection study and a silver/zinc release study, respectively (where $n = 1, 3, 5, 7, \ldots$). After each study, the substrate was immediately removed from the test solution, washed with DI water, dried with nitrogen gas purging and stored in a vacuum desiccator until the next use. Silver release studies were performed under similar reaction conditions in DI water devoid of any bacterial cells. Predetermined volume of samples was taken at regular intervals followed by acid digestion using dil. HNO_3 (0.1 M). After acid digestion, the samples were analyzed for silver and zinc released using ICP-AES. Standard solutions were used for the calibration. The time lag between disinfection and silver release studies was maintained as 10–12 hours in order to minimize the variability.

Mechanism of antibacterial action

To demonstrate the mechanism of the biocidal action of Ag/ZnO HNRs, *E. coli* cells (each at 10^6–10^7 CFU ml^{-1}) were treated with Ag/ZnO-20 substrate (2 × 2.3 cm^2) for 6 hours. Untreated *E. coli* cells were used as the control. The treated cells were harvested by centrifugation (5000 rpm, 10 min) and washed thrice with DI water to remove the loosely bound Ag or Zn over the bacterial surface. A series of pre-treatment steps were followed for electron microscopy analysis. Primary fixation of bacterial cells was achieved using 2.5% glutaraldehyde for 1 hour. After intermediate washing steps, secondary fixation was performed using 1% OsO_4 in the dark for 30 minutes. Phosphate buffer medium (pH 7.2) was used for washing the bacterial cells before and after the fixation steps. The samples were subsequently dehydrated with a graded ethanol series (30%, 50%, 70%, 90%, 95%, and 100%) followed by staining with 3% uranyl acetate. Bacterial cells were drop casted on carbon coated Cu grids and were air dried at room temperature for field emission gun-transmission electron microscopy (FEG-TEM) analysis. For field emission gun-scanning electron microscopy (FEG-SEM) analysis, bacterial cells loaded on Cu grids were examined without any conductive coating (gold/platinum/gold–palladium sputtering) to reduce possible artifact.

In vitro cytotoxicity and intracellular ROS generation

Human hepatocarcinoma cells (HepG2) were cultured in Dulbecco's modified Eagle's medium supplemented with 10% fetal bovine serum, 100 U ml^{-1} penicillin, 100 μg ml^{-1} strepto-

mycin, and 25 μg L^{-1} amphotericin-B in a 24-well plate. Cells (1×10^5 cells) were grown for 24 hours at 37 °C under a humidified atmosphere containing 5% CO_2/95% air. 3-(4,5-Dimethyl-thiazol-2-yl)-2,5-diphenyl tetrazolium bromide (MTT) assay was followed as reported earlier[27] with minor modifications. Before seeding the cells, Ag/ZnO-25 HNR substrates and pristine glass slides (without any Ag/ZnO deposition) of equal dimensions (1×1 cm^2) were sterilized by dipping in a 70% ethanolic solution for 2 hours followed by UV radiation for 30 minutes. A single Ag/ZnO HNR substrate (1×1 cm^2) was placed at the bottom of each well in the 24-well plate. HepG2 cells (200 μl in each well) were treated with Ag/ZnO HNRs for different time periods (6, 12, 24 and 48 hours) as four independent studies set up in triplicate. Control experiments were carried out using 1% Triton X-100 (positive control), which causes 100% toxicity to cells. Treated cells were subsequently incubated in MTT dye (1 mg ml^{-1}) for 4 hours in the dark. Cell viability was evaluated by the ability of metabolically active cells to reduce MTT to insoluble, purple formazan crystals. After incubation for the desired time period, the medium from each well was discarded and the resulting formazan crystals were dissolved in a 200 μl solution containing 10% sodium dodecyl sulphate and 0.01 N HCl. The absorbance was measured at 570 nm in a multi-well plate-reader (Bio-Tek, Winooski, USA). The percentage of viable cells was determined by the absorbance value of wells containing treated cells with those in untreated cells (negative control).

The intracellular ROS generation was determined using 2,7-dichlorofluorescein diacetate (DCFDA), a membrane permeable dye which undergoes hydrolysis by esterases present within the cells. The resulting deacetylated moiety is highly sensitive to react with various ROS (mainly peroxyl, hydroxyl and peroxynitrite anions) produced inside the cells and forms a fluorescent product, dichlorofluorescein (DCF). The intensity of fluorescence is therefore proportional to the amount of ROS produced by the cells. HepG cells (1×10^5 cells) were seeded in a 24-well plate (black bottom) for 24 hours. Similar to the MTT assay, grown cells were incubated with the Ag/ZnO-25 HNRs for 6, 12, 24 and 48 hours as four independent studies set up in triplicate. After treatment for the desired time period, the cells were washed thrice with PBS and were subsequently incubated in DCFDA dye (20 μM) for 30 minutes under dark conditions. To isolate the cells from solution, the reaction mixture was centrifuged at 2500 rpm for 10 minutes and the supernatant was discarded. The cells were redispersed in PBS (200 μl) and the fluorescence intensity was measured in a multi-well plate reader at excitation and emission wavelengths of 485 and 528 nm, respectively. The intracellular ROS level was expressed by the fold change in the mean fluorescence intensity of exposed cells with respect to the untreated cells.

3. Results and discussion

A hybrid antibacterial material was fabricated using ZnO nanorods (ZnO NRs). ZnO NRs serve as nano-reactors for *in situ* synthesis of silver nanoparticles concurrently providing a template for their subsequent immobilization using arginine as a linker. Arginine is known to bind silver ions *via* chelation and complexation mechanisms. Under alkaline conditions, arginine exists as a zwitterion and can form stable bidentate and tridentate complexes with silver.[25] It has been reported that bidentate complexes of silver–arginine exist in two possible forms.[22] First, Ag^+ coordinates with the carbonyl oxygen and with the nitrogen of the α-amino group, forming 'charge-solvated complexes'. Alternatively, Ag^+ is attached to the two oxygen atoms of the guanidino group of L-arginine forming 'salt bridge complexes'. Moreover, the presence of four nitrogen moieties in L-arginine and the formation of stronger Ag–N bonds to its side chain facilitate the formation of more stable silver–arginine tridentate complexes.[22,28]

Although amino acids are reported to reduce silver ions and form AgNPs, the introduction of silver nitrate into arginine solution did not cause any color change. Thus, the formation of AgNPs was not observed. Thus, it is hypothesized that Ag^+ undergoes complexation with the arginine molecule under mild alkaline conditions (pH 7–8), which lowers the standard redox potential of Ag^+/Ag, thus preventing the formation of AgNPs in solution.[17] We also observed that the introduction of arginine enhanced the stability of ZnO deposition on glass substrates and retarded the solubilisation of zinc under alkaline conditions. ZnO NRs grown on glass substrates were treated with an aqueous silver–arginine mixture of varying concentration (5–75 mM), followed by ascorbic acid mediated reduction. This resulted in a uniform deposition of AgNPs over the surface of ZnO NRs (Fig. 1).

Characterization

Different hybrid nanostructures (Ag/ZnO HNRs) synthesized using this approach were characterized to optimize the relative molar concentrations of $AgNO_3$ and arginine that would facilitate maximum immobilization of AgNPs on the ZnO surface. Preliminary results obtained through FTIR and Raman analyses (refer to section S3† and Fig. S1† in ESI) demonstrated the role of arginine as a linker molecule by the shift in the absorption spectrum of a few characteristic peaks and the enhancement in Raman signals. It was demonstrated that the incorporation of AgNPs did not affect the structural morphology and integrity of the ZnO surface. Moreover, the enhancement in Raman intensity can be extrapolated for qualitative determination of the extent of AgNP immobilization on various Ag/ZnO HNRs, which is primarily governed by arginine. Among various silver–arginine complexes, the mixture having 20 mM $AgNO_3$ concentration was expected to exhibit the most efficient immobilization of AgNPs on ZnO nanorods.

Based on a few recent studies,[29,30] it can be inferred that a stable silver–arginine interaction is favorable for immobilizing AgNPs on the ZnO template. Aliaga *et al.*[29] studied the extent of silver–arginine interactions in a colloidal solution using surface enhanced Raman spectroscopy (SERS) and reported a pH dependent conformational change in the structure of

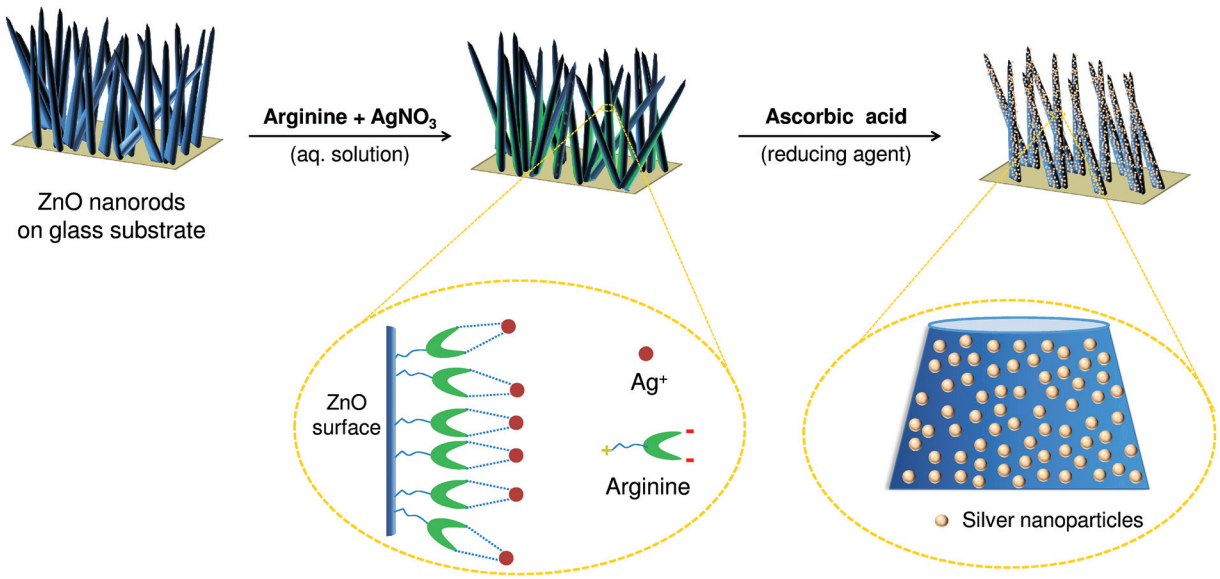

Fig. 1 Schematic representation of *in situ* synthesis and immobilization of silver nanoparticles on ZnO nanorods using arginine as a linker.

an arginine molecule. Thus, the stability of silver–arginine interactions is strongly dependent upon the solution pH. Garrido *et al.*[30] also studied the effect of pH on silver–arginine interactions using SERS and reported that the zeta potential of the complex mixture increased from −43.5 to −35.2 mV when the pH was increased from 7 to 9. The higher pH reduced the negative charge on arginine molecules so that the molecules become less hydrophilic, and thus induces a preferential and more stable silver–arginine interaction. In this study, the pH values of various silver–arginine solution mixtures were in the range of 7–10 and the pH of Ag/ZnO-20 was 8.6. Therefore, the best stability of Ag/ZnO-20 can be attributed either to the spatial orientation of arginine molecules or charge reduction on L-arginine molecules at pH 8.6, which may have contributed towards the most efficient silver–arginine interaction.

The quantitative estimation of Zn and Ag content on various samples, as obtained through ICP-AES analyses, is summarized in Table 1. For glass substrates of equal dimensions (2 × 2.3 cm^2), the average Ag loading increased up to Ag/ZnO-20 HNRs, while, for Ag/ZnO-25 and Ag/ZnO-75 HNRs, the silver loading drastically reduced. Since ZnO nanorods were grown by drop coating of ZnO seeds on the glass substrate, it was difficult to control the Zn content in each sample. Therefore, the mass ratio of Ag : Zn was taken as a parameter to determine the extent of silver immobilization on various ZnO–glass substrates. Calculated values indicate that the highest Ag : Zn ratio was obtained for Ag/ZnO-20 HNRs, validating the results obtained through FTIR and Raman analyses. In the case of Ag/ZnO-20 HNRs, the mass loading of silver was calculated to be 12.83 μg cm^{-2}, which is ~3.5-fold higher than in our previous study[7] where AgNPs were immobilized on a surface functionalized silica substrate. This is an indication of highly dense immobilization of silver nanoparticles on ZnO substrates. For all samples the amount of Zn deposition on the glass substrate was controlled in between 202 and 221 μg cm^{-2}. Using nitrogen sorption measurements, the specific surface area of Ag/ZnO-20 HNRs was found to be 57.1 m^2 g^{-1}. Compared to other Ag/ZnO hybrid nanorods, Ag/ZnO-20 HNRs demonstrated the best results on using this immobilization strategy and therefore they were used for further characterization and antibacterial studies as discussed in the following sections.

Table 1 ICP-AES analysis of ZnO nanorods loaded with various amounts of silver nanoparticles

Sample code	Zn content[a] (μg)	Ag content[a] (μg)	Ag : Zn	Ag loading (μg cm^{-2})
Pure ZnO	974 ± 55	0.0	0.000	0.00
Ag/ZnO-5	938 ± 61	8.1 ± 0	$0.009 \pm 5.4 \times 10^{-5}$	1.76
Ag/ZnO-10	959 ± 35	19.3 ± 3	$0.020 \pm 7.2 \times 10^{-4}$	4.20
AgZnO-20	1016 ± 91	59.0 ± 5	$0.058 \pm 1.2 \times 10^{-3}$	12.83
Ag/ZnO-25	1019 ± 36	31.2 ± 6	$0.031 \pm 1.6 \times 10^{-3}$	6.79
Ag/ZnO-75	964 ± 93	16.2 ± 2	$0.017 \pm 5.9 \times 10^{-4}$	3.52

[a] Average values based on three independent tests.

The extinction spectra were compared to characterize the effect of silver loading on the plasmonic properties of ZnO nanorods (Fig. 2a). Ag/ZnO HNRs showed a typical extinction spectrum in the visible region at about 440 nm due to the surface plasmon resonance of silver, which confirms that AgNPs were successfully immobilized over the ZnO surface. The formation of Ag/ZnO hybrid nanorods also caused a red shift (from 352 to 360 nm) in the extinction peak of ZnO as compared to pure ZnO nanorods. This was possibly caused by the strong interfacial coupling between immobilized AgNPs and ZnO, which is reported to reduce surface defects and promote charge separation.[31,32] Fig. 2b shows X-ray diffraction

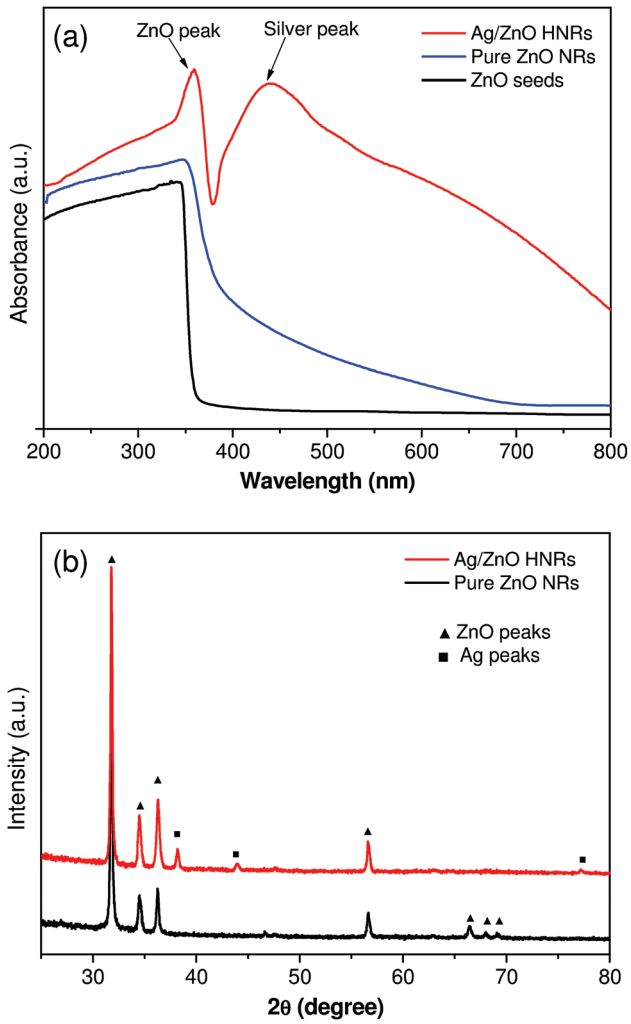

Fig. 2 UV-Vis extinction spectroscopy (a) and X-ray diffraction analysis (b) of pure ZnO and AgNP immobilized ZnO hybrid nanorods (HNRs).

(XRD) patterns of pure ZnO and AgNP-loaded ZnO HNRs. The diffraction peaks at 2θ = 31.8°, 34.5°, 36.3°, 56.6°, 66.4°, 67.9°, and 69.0° correspond to the (100), (002), (101), (110), (200), (112) and (201) planes, indicating the typical hexagonal wurtzite structure of ZnO nanorods (JCPDS card no. 36-1451). In the case of AgNP-loaded ZnO HNRs, the additional diffraction peaks at 2θ = 38.2° (111), 43.9° (200), and 77.2° (311) depicted the face centered cubic structure of AgNPs and demonstrated that all silver nanoparticles existed in their metallic (Ag^0) state. Moreover, since the immobilization of AgNPs did not cause any shift in the peaks of ZnO nanorods, this immobilization strategy helps in depositing AgNPs without altering the crystalline behavior of the ZnO material.

An X-ray photoelectron spectroscopy (XPS) analysis was performed to investigate the chemical states of Ag–ZnO hybrid nanorods (Fig. 3). The high resolution Zn 2p spectrum demonstrated two peaks at 1021.5 eV ($2p_{3/2}$) and 1044.5 eV ($2p_{1/2}$), which confirms the existence of zinc in Zn^{2+} form.[33] The high resolution Ag 3d spectrum of Ag–ZnO demonstrated two peaks at 367.5 eV (Ag $3d_{5/2}$) and 373.53 eV (Ag $3d_{3/2}$) with a peak splitting of 6.0 eV, which corresponds to metallic silver (Ag^0).[7] Interestingly, the immobilization of AgNPs on the ZnO template was evidenced through the decrease in the binding energy values of 3d doublet as compared to their standard values in bulk silver, *i.e.*, 368.2 eV and 374.2 eV, respectively.[18] The reduction in charge density occurred due to the transfer of electrons from Ag to the conduction band of ZnO at the interface, creating a new Fermi energy level for Ag–ZnO nanocomposite.[18,34] Similarly, peaks at 368.4 eV, 369.3 eV and 374.2 eV also suggest a strong association of silver with the oxygen and nitrogen moieties of arginine. A small fraction of these peaks can also be ascribed to AgO/Ag_2O species due to the formation of a thin oxide layer over AgNPs while the immobilized nanoparticles predominantly exist in their Ag^0 oxidation state. The formation of oxide layers over AgNPs is inevitable under ambient conditions.[35] It has been reported to facilitate controlled release of Ag^+ ions, which enhances the biocidal performance.[7,36]

As predicted, the high resolution O 1s spectrum showed a relatively complex pattern due to various associations of oxygen atoms with zinc, oxygen, and arginine biomolecule and therefore several possible peaks may coincide within a narrow range. The deconvoluted spectra showed a peak at 530.2 eV which can be assigned to the lattice oxygen (O^{2-}) in ZnO.[34,37] A sharp peak at 531.3 eV provides sufficient indication of the Ag–O bond formation in the hybrid nanocomposite, while a smaller proportion of AgO/Ag_2O is also reported to exist within this region.[7] The presence of arginine over ZnO nanorods was further confirmed through the peaks at 532.9 eV which can be assigned to C–OH, C–O, and C═O bonds available for silver ions to bind with.[38] Besides this, the peak at the 532–533 region is also attributed to the oxygen associated with the surface hydroxyl groups of ZnO.[33] There was also a small component peak of 535 eV which was ascribed to several associations of oxygen atoms present in the arginine moieties.[39] Arginine being the only source of carbon and nitrogen, the appearance of carbon and nitrogen spectra in the Ag/ZnO HNRs clearly indicates the existence of arginine over the ZnO surface. The high resolution C 1s spectra were deconvoluted into three distinct peaks that correspond to the C–C bond (285.7 eV), and the carbon atoms bonded to different functional moieties of arginine (C–O/C–N at 286.3 eV; and C═O/O–C═O at 290 eV).[40–42] Similarly, the N 1s spectra can be deconvoluted into three distinct peaks at 399.2 eV (C–N bond), 400.4 eV (C═N bond) and 400.7 eV (protonated amine, NH_3^+).[41]

Analyzing Ag/ZnO HNRs using FEG-SEM, it was noticed that ZnO nanorods were randomly aligned throughout the glass substrate, while AgNPs were observed as white dotted structures throughout the surface of the ZnO nanorods (Fig. 4a inset). A bunch of ZnO rods with immobilized AgNPs suggested that multiple nanorods may have grown from a single aggregate of ZnO seed during the growth process (Fig. 4b). The elemental composition of the sample was studied by energy-dispersive X-ray (EDX) analysis. As shown in Fig. 4c (inset), the presence of zinc, oxygen and silver peaks appeared due to Ag/ZnO

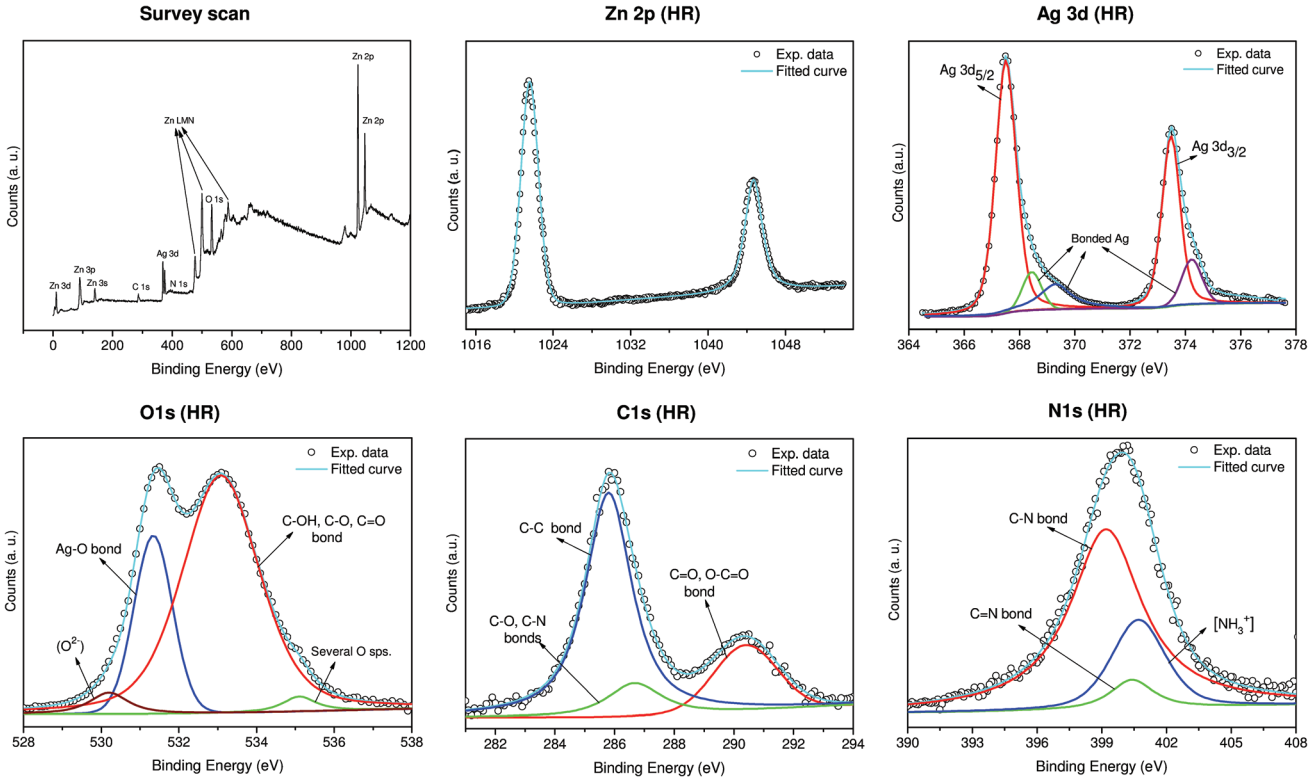

Fig. 3 XPS spectral analysis of Ag/ZnO hybrid nanorods showing full scan and corresponding deconvoluted peaks in the high resolution (HR) spectra of various elements present, *i.e.,* Zn (2p), Ag (3d), O (1s), C (1s), and N (1s).

hybrid nanostructures, while a peak of silicon was observed because of the glass (silica) material used as the support matrix. A smaller proportion of arginine was also evidenced through a relatively smaller peak of carbon, whereas no nitrogen peak was identified due to insufficient element counts during the course of EDX analysis. The elemental mapping analysis for a selected region (indicated in pink) clearly showed that silver (green) is homogeneously distributed throughout the surface in addition to other major elements, *i.e.*, Zn (blue), O (white) and Si (red). Semi-quantitative estimation of the surface composition indicated that nearly 30% (by wt.) of the surface is occupied by elemental silver (see Table S1† in ESI). The absence of any other peaks clearly indicates that the synthesized antibacterial substrate is in pure form, thus validating an efficient immobilization of AgNPs using our greener approach.

Transmission electron microscopy (FEG-TEM) was performed to confirm the immobilization of AgNPs on the ZnO surface (Fig. 5). The results obtained corroborate with those of the FEG-SEM analysis, where silver nanoparticles were found to be evenly distributed over ZnO nanorods (Fig. 5a). Analyzing the TEM micrographs of the ZnO surface (side view) it was evident that immobilized AgNPs were nearly spherical in shape with size ranging from 5 to 14 nm (Fig. 5b). The average size of AgNPs was found to be ~11 nm. The HRTEM micrograph (Fig. 5c) reveals a distinct interface and spatial arrangement of atoms between AgNP and ZnO. The lattice fringes having a *d*-spacing of 0.26 nm and 0.24 nm correspond to the crystallographic (002) plane of zinc and the (111) plane of the face centered cubic AgNPs,[34] respectively (Fig. 5d and e). The selected area diffraction (SAED) analysis further validates the presence of silver and zinc in Ag/ZnO HNRs due to their characteristic diffraction patterns.

Antibacterial studies

It is worth mentioning that immobilizing AgNPs onto another bactericidal material, *i.e.*, ZnO, may promote synergistic action and may cause a superior antibacterial effect compared to AgNPs and ZnO, each acting individually. In order to elucidate this, the antibacterial performances of three different antibacterial materials, *i.e.*, pure ZnO NRs, colloidal AgNPs (average size, 10 ± 2 nm), and AgNP-silica substrate, were compared with Ag/ZnO HNRs against *E. coli* MTCC 443 strain at an initial cell count of 10^3–10^4 CFU ml^{-1} in a 100 ml batch reactor. As shown in Fig. 6a, the Ag/ZnO hybrid nanorods showed much faster antibacterial activity than pure ZnO nanorods and achieved 100% bactericidal activity in 30 minutes. In contrast to this, pure ZnO nanorods could not achieve complete bactericidal activity even after a much longer duration, *i.e.*, 120 minutes. Although the colloidal AgNPs showed promising bactericidal potential compared to the pure ZnO nanorods, the time to achieve complete disinfection was prolonged to 90 minutes. The AgNP-silica substrate also demonstrated inferior bactericidal effect (50 minutes) when compared to Ag/ZnO HNRs, which can

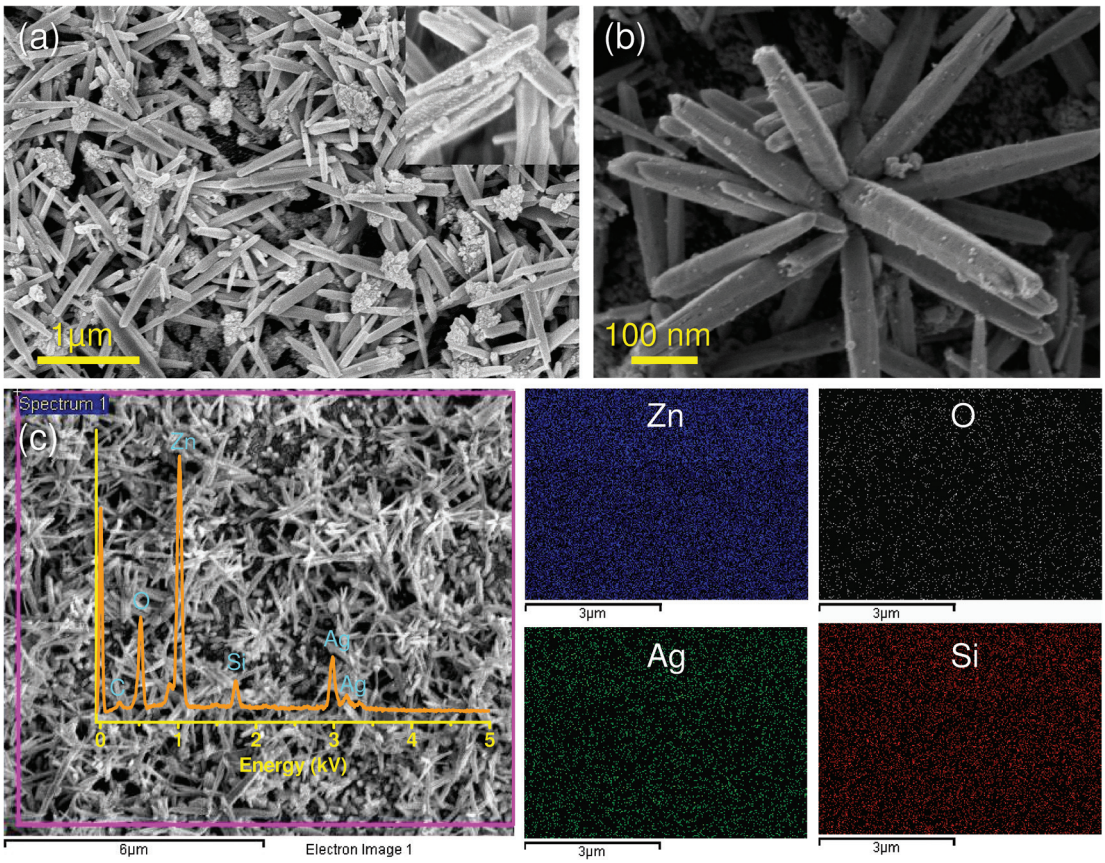

Fig. 4 FEG-SEM micrographs showing (a) uniform deposition of Ag/ZnO nanorods on the glass substrate. Image in the inset reveals a high deposition of silver nanoparticles. (b) Bunch of ZnO nanorods with immobilized AgNPs. (c) Elemental mapping done for the selected region revealed the presence of zinc (Zn, blue), oxygen (O, white), silver (Ag, green) and silicon (Si, red). Surface composition of the substrate was based on an EDX analysis, with the characteristic peak of silver at ~2.9 kV in addition to other elements.

be explained on the basis of ~3.5 higher silver loading in the case of the latter. Analyzing these data, it can be predicted that the hybrid nanocomposite of AgNP and ZnO acts effectively against *E. coli*, resulting in enhanced antibacterial performance compared to the individual components.

Zone of inhibition (ZoI) tests were performed to compare the bactericidal potential of the two substrates in a solid medium (Fig. 6b). The results were in good agreement with those in the liquid medium where superior bactericidal activity of Ag/ZnO HNRs was marked by a noticeable ZoI formation. Pure ZnO NRs did not show a distinct inhibition zone. Fuchs and Tiller[43] demonstrated similar results where an antibacterial substrate depicted a distinct but narrow ZoI due to its contact-killing mechanism. The narrow width of the ZoI indicated that bacteria were able to grow in close proximity to the substrate since there was negligible release of biocidal material from the antibacterial substrate. Furthermore, in order to verify its contact-killing bactericidal action, it was observed that the Ag/ZnO HNR-glass substrate not only killed bacterial colonies in that area but also suppressed further growth of bacteria at that zone even after 24 hour incubation, owing to its 'bacteriostatic' effect (see Fig. S2† in ESI). Similar photographic images have been shown in an earlier study,[44] where AgNP coated cellulose acetate fibers when placed in direct contact with a bacterial lawn for 4 hours showed complete inhibition of *E. coli* growth at the contact area. Thus, although a dual mode of antimicrobial action of Ag/ZnO HNRs is envisaged, the contact-killing mode as opposed to inactivation through release of silver ions is predominantly responsible for the antimicrobial activity. However, some diffusion of biocidal material from the immobilized substrate and its contribution towards antibacterial action cannot be ruled out.

Previous studies have demonstrated a substantial difference in bactericidal activity of antimicrobial material, if either the type of culture strain or the initial bacterial concentration is varied.[7,8,26,45] To investigate the wide-spectrum antibacterial activity of Ag/ZnO HNRs, *E. coli* MTCC 443 and *B. subtilis* MTCC 441 strains were selected as model Gram (–) and Gram (+) strains. Four independent tests were performed against each of the strains, in deionized water (DI) and phosphate buffer medium (PBS), both at lower (10^3 CFU ml^{-1}) and higher (10^5 CFU ml^{-1}) initial cell concentrations (Fig. 7). Ag/ZnO HNRs demonstrated good antibacterial activity against both types of strains where complete disinfection could be achieved within 70 minutes for all the test conditions. In DI water, it took 30 and 60 minutes for complete disinfection against

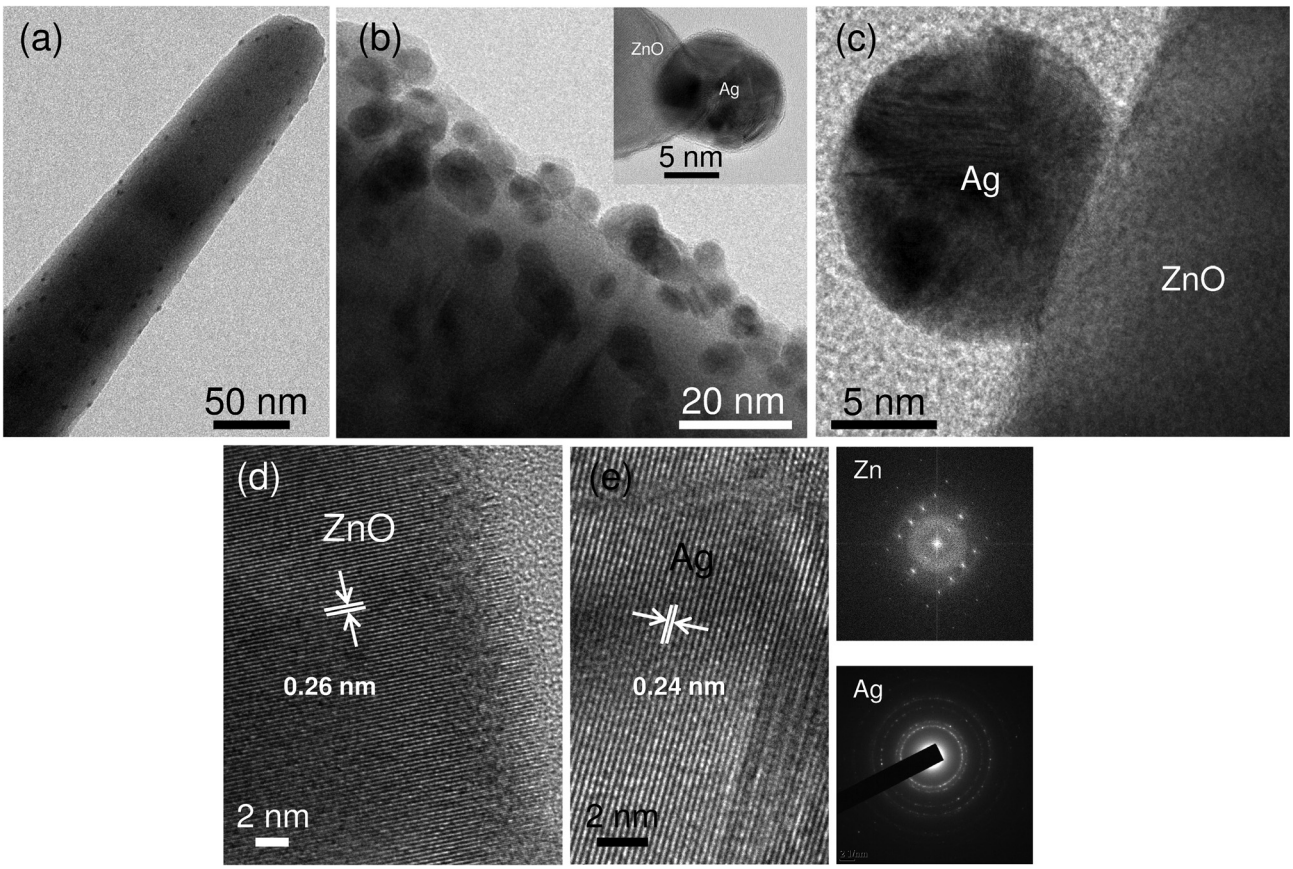

Fig. 5 FEG-TEM micrograph of (a) a single ZnO nanorod with uniform immobilization of silver nanoparticles. (b) Side view of Ag/ZnO nanorods and immobilized AgNP at the tip of ZnO (inset). HRTEM image (c) showing a distinct interface between Ag and ZnO. High resolution micrographs of ZnO (d) and silver nanoparticles (e) with characteristic *d*-spacing and corresponding diffraction patterns of ZnO (above panel) and silver (below panel) are also presented.

E. coli at 10^3 and 10^5 CFU ml^{-1} initial bacterial counts, respectively. Under similar test conditions, the time to achieve complete disinfection was marginally delayed to 40 and 70 minutes against *B. subtilis* strain, showing the strain-specific bactericidal activity of Ag/ZnO hybrid nanorods. As compared to DI water, no significant variation in the antibacterial activity of Ag/ZnO HNRs was observed in the phosphate buffer medium, which mimics the physiological conditions. Therefore, the AgNP immobilized ZnO substrate can be well suited for other potential *in vitro* applications, such as surgical coatings and wound dressings.

Antibacterial efficacy on multiple reuse

Nanocomposites, which act as an immobilizing matrix and/or support for antibacterial agents, are advantageous as they enable not only the convenient use of the antibacterial agents but also facilitate their release.[5] However, the antibacterial activity of such materials is adversely affected due to the continuous depletion of Ag^+ ions, rendering them unsuitable for long term use. One of the aims of the current study was to elucidate the antibacterial efficacy of Ag/ZnO HNRs on multiple reuse and to determine the corresponding silver and zinc release. As shown in Fig. 8a, the Ag/ZnO HNRs remained bactericidal against *E. coli* MTCC 443 (10^3 CFU ml^{-1}) even after the same substrate was reused eleven times. Initially, up to the 5^{th} reuse, the time for complete killing remained constant at 30 minutes although the rate of kill was slower in the initial phase. For subsequent use, *i.e.*, $7^{th}/9^{th}$ and 11^{th} reuse, the time to achieve complete disinfection using Ag/ZnO HNRs was increased by 5 and 10 minutes, respectively. Silver release after 90 minutes duration for the 2^{nd}, 4^{th}, 6^{th}, 8^{th}, and 10^{th} use was 103.8 ± 4.6, 94.7 ± 2.5, 65.2 ± 2.8, 44.7 ± 2.5, and 40 ± 1.1 ppb, respectively (Fig. 8b). As predicted, the decrease in the disinfection kinetics can easily be explained on the basis of lower silver release with every subsequent use. Interestingly, as low as ~26 ppb (11^{th} use, 30 min) of silver release was sufficient to elicit 100% killing of *E. coli* cells after multiple reuse. It was also essential to study whether the amount of Zn^{+2} release from the ZnO nanorods over repeated use contributed towards the enhanced bactericidal action of Ag/ZnO HNRs. Fig. 8c shows that the amount of Zn release after 90 minutes was progressively reduced from 91.6 ± 2.4 ppb in the 2^{nd} use to 18.5 ± 0.2 ppb after the 8^{th} reuse. For subsequent uses, zinc release was not detected (below the detection limit). The variation in the release profile of silver and zinc in the aqueous phase can be explained on the basis of their different chemical states.[19]

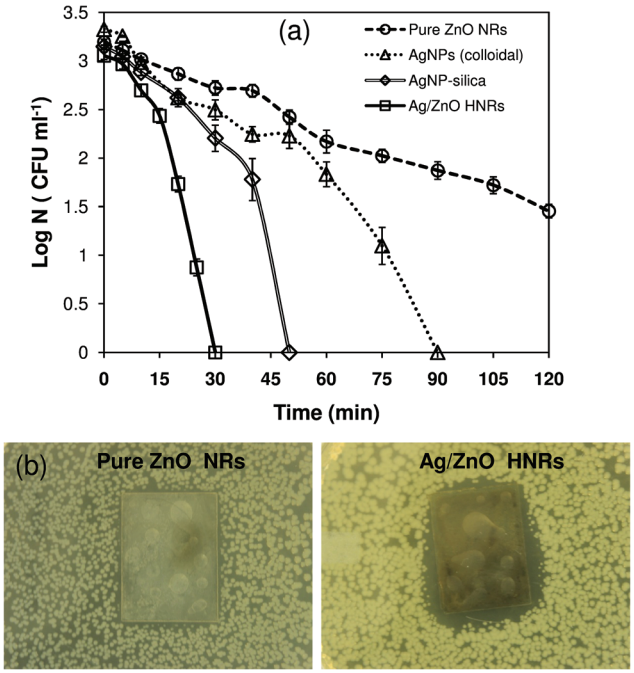

Fig. 6 (a) Comparative disinfection potential of pure ZnO nanorods, AgNP immobilized ZnO nanorods (Ag/ZnO HNRs) and colloidal AgNPs (12 ± 2 nm, 6.0×10^{-2} mg in mass). All disinfection studies were performed using *E. coli* MTCC 443 strain (initial cell concentration, $\sim 10^3$ CFU ml^{-1}) in a 100 ml batch reactor. (b) Zone of inhibition (ZoI) tests done at relatively higher bacterial counts (10^5–10^6 CFU ml^{-1}) showing the bacteriostatic effect of Ag/ZnO HNRs, while no ZoI was observed in the case of pure ZnO nanorods.

Silver, present in their nanoparticulate form (Ag^0), is considered to be more reactive than the oxide form of zinc (ZnO), which may lead to higher release of silver, both in the form of silver ions as well as AgNPs. Despite this, it was observed that the amount of silver and zinc release over 30 minutes (*i.e.*, time for complete disinfection) with every use was well below the permissible concentration limits for Ag (*i.e.*, 100 ppb) and Zn (*i.e.*, 3–5 ppm) in potable water, as defined by the World Health Organization.[20] Therefore, it can be predicted that the Ag/ZnO HNRs would pose minimum health risks. Low discharge of the biocidal materials would also minimize adverse effects on other organisms in the ecosystem.

The disinfection profile and silver/zinc release profiles on multiple reuse also gave useful insights to determine the mechanism of antibacterial action of Ag/ZnO HNRs. As the results indicated, the continuous depletion of silver and zinc ions did not significantly affect the extent of disinfection with every usage. This implies that the mode of bactericidal action of Ag/ZnO HNRs cannot be fully explained on the basis of release of silver and zinc only. Rather, the immobilized Ag/ZnO HNRs may act primarily through a contact-killing mode. In our recent study,[7] it was illustrated that immobilized AgNPs demonstrated bactericidal action predominately *via* direct contact-killing mode, while release of silver ions had a minimum role in disinfection. In this study, the extent of disinfection remained the same irrespective of significant reduction (~37%) in silver release after the 2nd to 6th reuse, indicating the role of direct contact in bacterial killing. Interestingly, release of zinc ions appeared to have no significant effect on the bactericidal performance since there was only a marginal delay in achieving complete disinfection after the 10th reuse, where zinc release was not even detected. This showed that Ag/ZnO HNRs could retain their antibacterial efficacy and were unaffected by the absence of zinc ions in the releasing medium. These results preclude our initial hypothesis regarding the synergistic role of zinc and silver nanoparticles in the antibacterial action of Ag/ZnO HNRs. In contrast to this, the ZnO template seems to contribute primarily by providing a high surface area for the deposition of AgNPs, thereby facilitating the direct-contact mode of action of immobilized AgNPs. Therefore, the enhanced antibacterial action of the Ag/ZnO substrate can be better described by a dual mode of bactericidal action, *i.e.*, direct contact killing upon contact of bacteria with Ag/ZnO HNRs and leaching of silver in a nanoparticulate and/or ionic form.

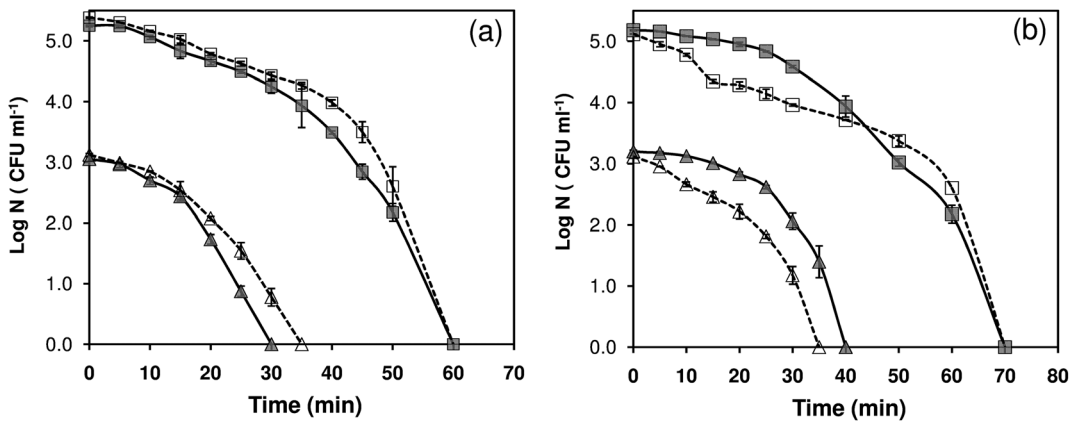

Fig. 7 Strain-specific antibacterial activity of Ag/ZnO hybrid nanorods (2×2.3 cm^2) against (a) Gram-negative, *E. coli* MTCC 443 and (b) Gram-positive, *B. subtilis* MTCC 441 strain. For each strain, disinfection kinetics was tested at an initial concentration of 10^3 CFU ml^{-1} (triangle) and 10^5 CFU ml^{-1} (square) in both deionized water (continuous line) and phosphate buffer medium (dashed line).

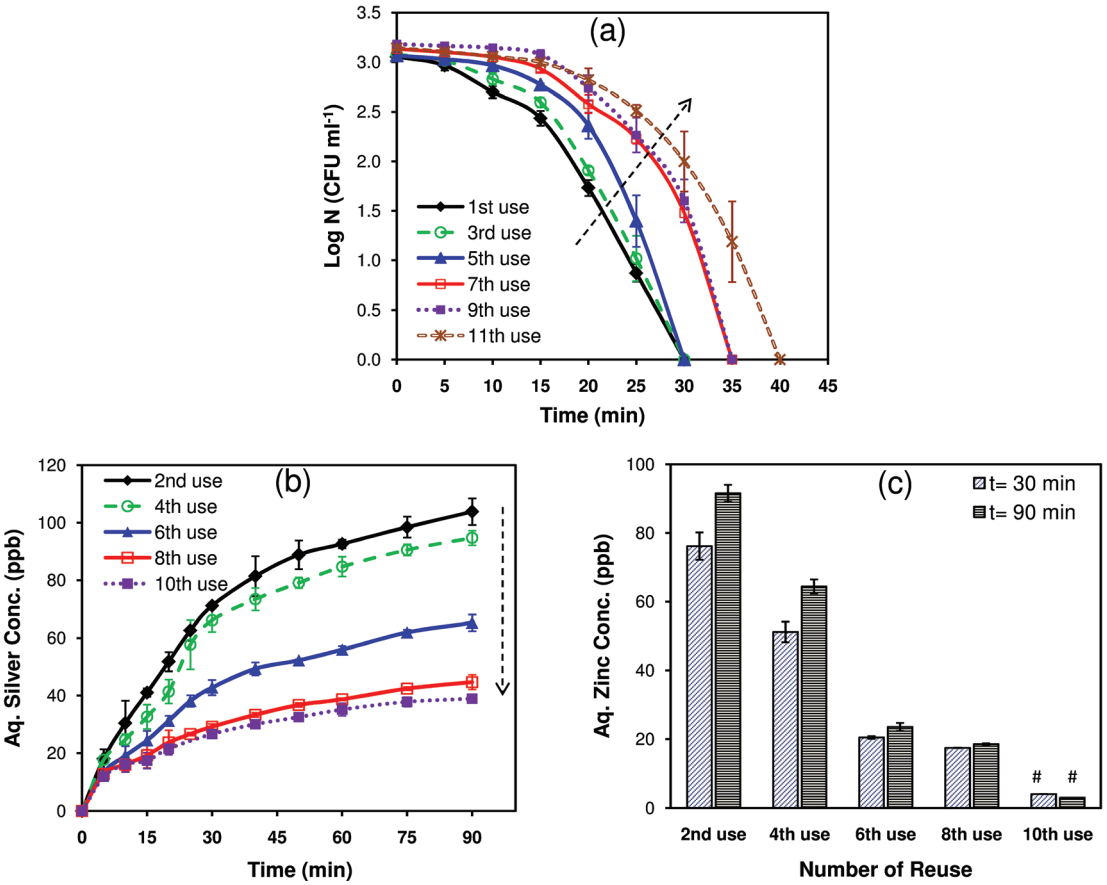

Fig. 8 (a) Disinfection performance of a single Ag/ZnO HNR substrate (2 × 2.3 cm^2) after 11 times repeated usage against *E. coli* MTCC 443 (10^3 CFU ml^{-1}). (b) The corresponding silver release profile after every usage was evaluated. (c) Zinc release after each use over 30 min and 90 minutes duration. (# below the detection limit.)

E. coli–Ag/ZnO interaction

In order to further investigate the interaction behaviour of the AgNP/ZnO substrate with the bacterial cells, SEM and TEM imaging was done (Fig. 9). Ag/ZnO HNR treated *E. coli* cells showed adverse effects as compared to untreated cells (see Fig. S3a† in ESI), and significant population of AgNPs was observed inside the bacterial cells (Fig. 9a). The presence of AgNPs near the cell membrane and inside the cells is considered to be the most fundamental and accepted mechanism for the antibacterial action of AgNPs other than silver ion release.[46,47] AgNPs were located both at the periphery of the cell membrane as well as deep within the cells as aggregates with a peculiar pattern (Fig. 9b). Similar patterns of AgNP aggregates have been evidenced in an earlier study, where the role of bacterial surface proteins was found to be critical for AgNP binding and aggregation pattern formation.[48] Therefore, it can be hypothesized that during earlier stages of bacteria–AgNP interaction, the presence of surface proteins facilitated the formation of AgNP aggregates and mediated their subsequent entry into the intracellular environment *via* endocytosis (Fig. 9c). After successful internalization, AgNP aggregates could be translocated inside the bacterial machinery to carry out antibacterial action through multiple mechanisms, such as ROS generation, blocking cell respiration and inhibiting DNA replication. These mechanisms may work concurrently and mediate the enhanced antibacterial effect. While assessing the Ag/ZnO–*E. coli* interactions, the presence of crystalline form (Fig. 9e) and the appearance of the characteristic peak at ~2.9 kV during EDX analysis (see, Fig. S3b† in ESI) supported the existence of AgNPs (*i.e.*, Ag^0) in bacterial cells. In contrast to this, crystalline Zn was not detected in any of the treated bacterial cells. Thus, its role in antibacterial action was not mediated *via* zinc nanoparticles. The release studies have also shown the negligible role of zinc ions. The antibacterial action was mediated by silver both in the form of AgNPs and silver ions.

Based on FEG-SEM analysis, some other possible mechanisms of bactericidal action may be hypothesized. As shown in the micrograph (Fig. 9e), Ag/ZnO HNR treated cells appeared to show atypical shape and a few cells were severely damaged (encircled). Membrane disruption may increase the cell permeability and allow intracellular material to come out, ultimately causing cell death (Fig. 9e, the inset above).[49] The formation of pits and holes on the bacterial surface indicates cell damage, which consequently allows the internalization of

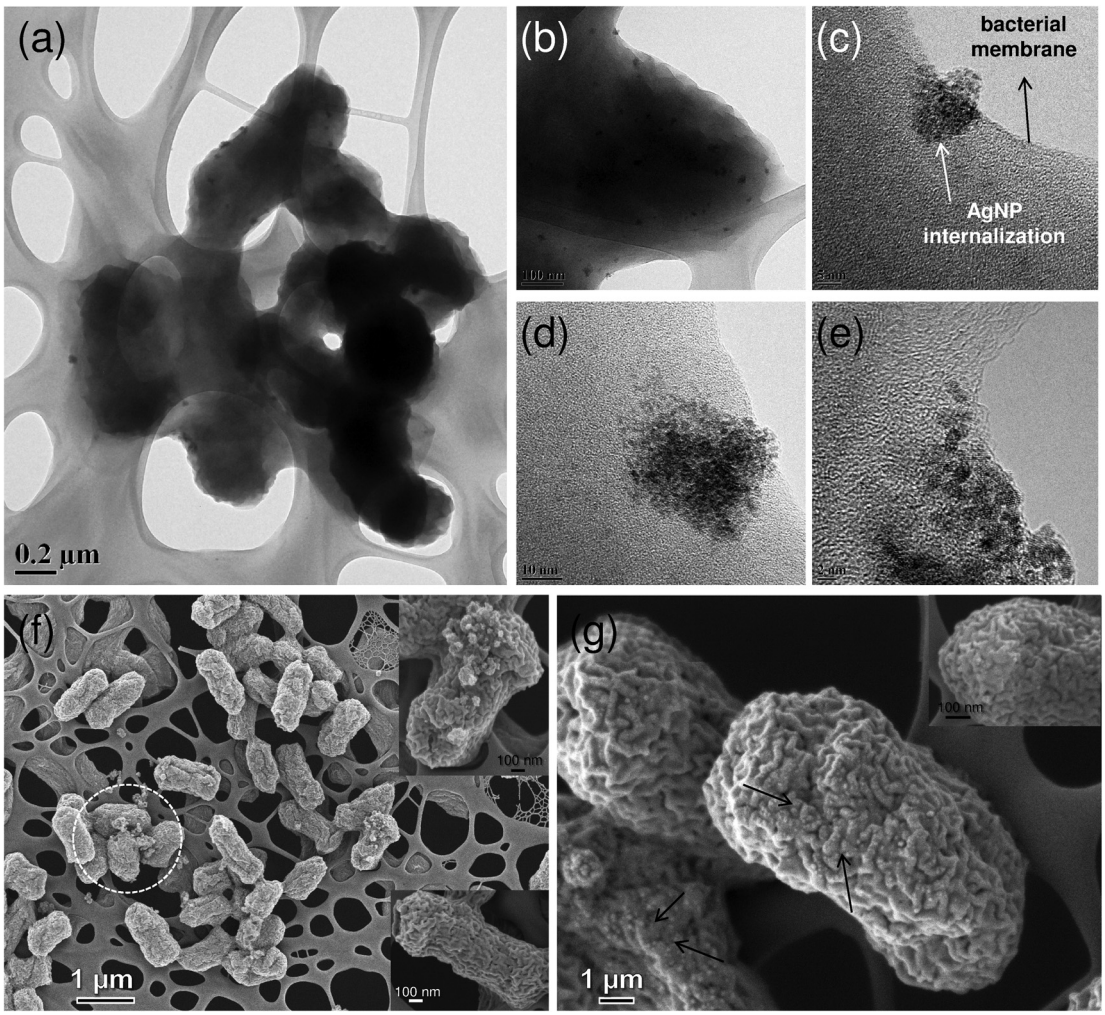

Fig. 9 FEG-TEM (a–e) and FEG-SEM (f, g) analyses of *E. coli* cells (bacterial count, 10^6–10^7 CFU ml^{-1}) treated with Ag/ZnO HNR loaded substrate. (a) Lower and (b) higher magnification showing the presence of AgNPs, both near the cell membrane and in the interiors of bacterial cells. (c) An early and (d) late stage of internalization of AgNP aggregates (white arrow) near the cell membrane (black arrow). (e) Crystalline structure reveals the presence of silver in its Ag^0 state, *i.e.*, AgNPs. SEM images of (f) damaged *E. coli* cells with ruptured morphology (inset, above) and formation of pits and holes on the bacterial surface (inset, below). (g) Silver nanoparticles were homogeneously present all over the surface of bacterial cells.

AgNPs (Fig. 9e, the inset below).[26] We also observed that AgNPs were not only present inside the bacterial cells; they were universally present over the entire bacterial surface (Fig. 9f). The interaction of AgNP/ZnO with bacterial cells leads to multiple pathways for bactericidal action, where it is extremely difficult to analyze which mechanism predominates over another. It can be assumed that an initial AgNP–bacterial interaction plays an important role. The results clearly indicate that the hybrid nanocomposite containing AgNPs and ZnO is a promising candidate for antibacterial applications owing to its dual mode of antibacterial action, contact-killing and release of metal ions.

Cytotoxicity analysis of human HepG2 cells

The use of nanomaterials containing silver and zinc oxide is often limited for therapeutic purposes owing to their intrinsic cytotoxic effects on humans.[50] A few recent studies have shown that the immobilization of AgNPs onto a substrate matrix would limit the release of silver in aqueous medium thereby causing either minimal toxic effects or none at all on mammalian cells.[51–54] Agarwal *et al.*[51] demonstrated that AgNPs immobilized on polyelectrolyte multilayer (PEM) films of poly(allylamine hydrochloride) and poly(acrylic acid) did not induce any cytotoxic effects against the mouse fibroblast cell line, NIH-3T3, under various test conditions. Beside this, AgNP-impregnated PEMs showed good antibacterial activity against *Staphylococcus epidermidis*, a clinical isolate from a veterinary hospital. In a different study, poly(L-glutamic acid)-capped silver nanoparticles were encapsulated within poly(lactide-*co*-glycolide) nanoparticles, which showed superior antibacterial activity against seven pathogenic strains without affecting the cell viability of the human HepG2 cells.[54] Therefore, it is quite possible to construct non-cytotoxic, AgNP-based antibacterial substrates by exploring some effective

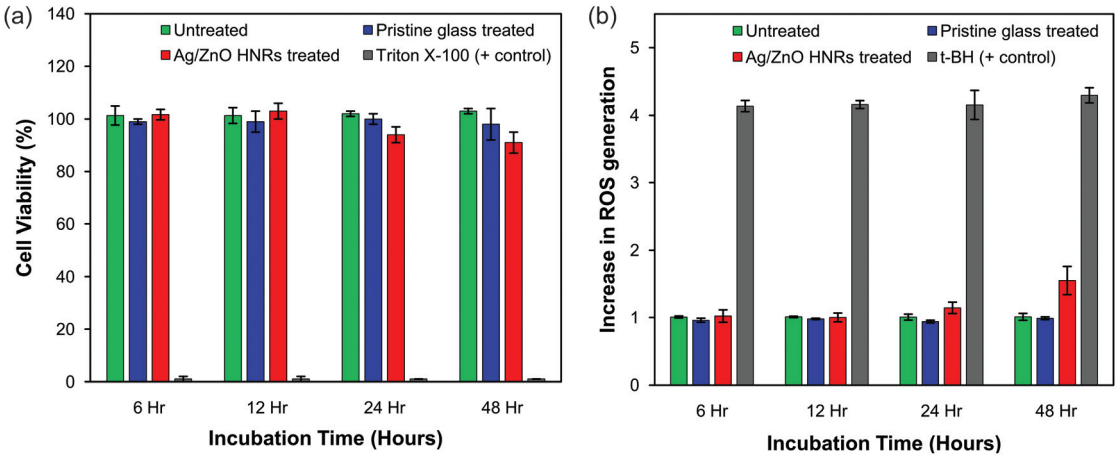

Fig. 10 Cytotoxicity analysis of Ag/ZnO hybrid nanorods on human hepatocarcinoma (HepG2) cells as determined by (a) an MTT assay and (b) intracellular ROS generation. Cells were treated with Ag/ZnO HNRs deposited on the glass substrate (1 × 1 cm^2) and the pristine glass substrate (1 × 1 cm^2) for various time periods, and (a) the percentage of cell viability and (b) the intracellular ROS levels were evaluated after each treatment. Triton X-100 and tertiary butyl hydroperoxide (t-BH) were taken as a positive control for MTT and ROS determination experiments, respectively. Experiments were performed in triplicate; data shown are expressed as mean ± standard error.

immobilization strategies, which can control silver release into the medium to an amount just sufficient to cause bactericidal effects.

In order to establish the fact that Ag/ZnO HNRs exhibit an enhanced, long-term antibacterial efficacy and do not cause undesirable toxic implications on human cells, cytotoxicity experiments were performed against HepG2 cells through the MTT assay. HepG2 cells are considered to be a useful *in vitro* model for the detection of cytotoxic and genotoxic agents.[55] As shown in Fig. 10a, cell viability of HepG2 cells treated with Ag/ZnO-25 HNRs were tested at four different time periods, *i.e.*, 6, 12, 24 and 48 hours. Compared to untreated cells (negative control), cells treated with Ag/ZnO HNRs did not show any significant reduction in cell viability even after 24 hours of incubation. The pristine glass substrate did not contribute towards any cytotoxic effects and showed similar cell viability as that with the Ag/ZnO HNRs. As a positive control for toxicity, cells treated with Triton X-100 showed complete absence of cell viability. Under the given test conditions, Ag/ZnO HNRs showed no cytotoxic effects on human cells, which is indicative of good biocompatibility of the hybrid nanocomposite. Moreover, we can interpret its minimal toxicological consequences on aquatic organisms, due to low discharge of silver and zinc from the immobilizing template. The silver loading in Ag/ZnO HNRs (1 × 1 cm^2) was calculated to be 2.8 μg cm^{-2}, which is nearly ~10-fold lower (25 μg cm^{-2}) than that reported by Shi *et al.*[53] where AgNPs were immobilized on the PEM functionalized stainless steel surface. Even at a much higher AgNP loading, Shi *et al.*[53] did not find any cytotoxic effects on mammalian cells. Thus, Ag/ZnO HNRs do not provoke cytotoxic responses to human cells and yet demonstrated excellent antibacterial efficacy.

A number of studies have proposed sub-lethal effects of AgNPs and nano-ZnO, when present either in very low concentration or short incubation times,[56,57] due to the generation of intracellular reactive oxygen species (ROS). Higher production of intracellular ROS can induce severe oxidative stress and is considered to be one of the most important mechanisms for cellular apoptosis, due to nanomaterial exposure.[58] To determine whether the interaction between Ag/ZnO hybrid nanorods and HepG2 cells would lead to oxidative stress, we measured the intracellular ROS generation using the DCFDA assay. As shown in Fig. 10b, no significant increment in ROS generation was noticed up to 24 hours, as compared to the untreated cells. A relatively longer period of treatment (*i.e.*, 48 hours) may cause some sub-toxic effects on cells, as indicated by a slight increase in the ROS level. The positive control, tertiary butyl hydroperoxide (t-BH), induced a 3.2-fold increase in ROS generation as compared to the untreated cells. These results are in contrast to earlier studies, where AgNPs and ZnO nanoparticles have been reported to induce severe oxidative stress to cells both by their "nanoparticulate" effect as well as the release of ionic forms.[59–62] It was therefore anticipated that probably the intrinsic chemical composition of Ag/ZnO hybrid nanorods could have an inhibitory effect on ROS generation. Interestingly, L-arginine, one of the components of Ag/ZnO HNR synthesized in this study, has been reported to act as a free radical scavenger and possesses antioxidant properties.[63] Tripathi *et al.*[64] also reported the use of L-arginine as an oral supplement to patients suffering from acute myocardial infarction, as it retards ROS production by scavenging the oxygen derived free radicals. Stevanovic *et al.*[54] have recently demonstrated the ROS scavenging property of ascorbic acid, another antioxidant molecule whose presence made the AgNP-loaded material highly bactericidal without causing cytotoxic effects on HepG2 cells. Therefore, it is expected that the presence of arginine not only facilitated dense immobilization of AgNPs on ZnO nanorods, but could

also inhibit the ROS-induced cytotoxicity to some extent. Further tests will be required to determine their sub-lethal, genotoxic effects in detail.

4. Conclusions

In this study, we have demonstrated a facile, inexpensive and entirely green approach for immobilization of silver nanoparticles on a ZnO nanotemplate. The presence of arginine not only facilitates a highly localized assembly of AgNPs, but also enhances the stability of ZnO deposition on the glass matrix and reduces the potential toxicity by limiting the release of zinc ions under alkaline conditions. The Ag/ZnO hybrid nanomaterial was found to be extremely stable in aqueous medium and showed an extraordinary bactericidal effect against both Gram-positive and Gram-negative bacterial strains. The results obtained through zone of inhibition (ZoI) studies and surface contact tests also depict growth inhibition of bacterial cells (*i.e.*, bacteriostatic effect). The Ag/ZnO HNRs acted primarily through direct contact killing mode and released very low concentrations of silver and zinc in the aqueous medium, thus minimizing potential health risks and other adverse effects associated with their discharge. Cytotoxicity results clearly indicate that Ag/ZnO HNRs deposited on glass substrates do not induce cytotoxic effects on the human cell line, but retain antibacterial efficacy even after multiple reuse. This immobilization strategy therefore holds good promise and enormous potential to be exploited for various antibacterial coatings in implantable biomaterials and surgical instruments.

Acknowledgements

The authors gratefully acknowledge the Sophisticated Analytical Instrument Facility (SAIF) and the IIT-Bombay central facility (XRD, ICP-AES, XPS and FEG-TEM) for characterization studies. We also acknowledge the Department of Chemical Engineering, IIT Bombay for the BET measurement test. This study was partially funded by Nanomission, DST, Govt of India.

References

1 S. Chernousova and M. Epple, *Angew. Chem., Int. Ed.*, 2013, **52**, 1636.
2 M. J. Hajipour, K. M. Fromm, A. Akbar Ashkarran, D. Jimenez de Aberasturi, I. R. d. Larramendi, T. Rojo, V. Serpooshan, W. J. Parak and M. Mahmoudi, *Trends Biotechnol.*, 2012, **30**, 499.
3 A. Ivask, A. ElBadawy, C. Kaweeteerawat, D. Boren, H. Fischer, Z. Ji, C. H. Chang, R. Liu, T. Tolaymat, D. Telesca, J. I. Zink, Y. Cohen, P. A. Holden and H. A. Godwin, *ACS Nano*, 2013, **8**, 374.
4 Q. H. Tran and A. T. Le, *Adv. Nat. Sci.: Nanosci. Nanotechnol.*, 2013, **4**, 033001.
5 M. Lv, S. Su, Y. He, Q. Huang, W. Hu, D. Li, C. Fan and S. T. Lee, *Adv. Mater.*, 2010, **22**, 5463.
6 C. Tang, W. Sun and W. Yan, *RSC Adv.*, 2014, **4**, 523.
7 S. Agnihotri, S. Mukherji and S. Mukherji, *Nanoscale*, 2013, **5**, 7328.
8 S. Mukherji, J. Ruparelia and S. Agnihotri, in *Nano-Antimicrobials: Progress and Prospects*, ed. N. Cioffi and M. Rai, Springer-Verlag, Berlin, Heidelberg, 2012, p. 225.
9 S. Agnihotri, S. Mukherji and S. Mukherji, *Appl. Nanosci.*, 2012, **2**, 179.
10 N. Perkas, G. Amirian, G. Applerot, E. Efendiev, Y. Kaganovskii, A. V. Ghule, B. J. Chen, Y. C. Ling and A. Gedanken, *Nanotechnology*, 2008, **19**, 435604.
11 M. Moritz and M. Geszke-Moritz, *Chem. Eng. J.*, 2013, **228**, 596.
12 P. Dallas, J. Tucek, D. Jancik, M. Kolar, A. Panacek and R. Zboril, *Adv. Funct. Mater.*, 2010, **20**, 2347.
13 Z. Li, H. Tang, W. Yuan, W. Song, Y. Niu, L. Yan, M. Yu, M. Dai, S. Feng and M. Wang, *Nanotechnology*, 2014, **25**, 145702.
14 I. Ocsoy, M. L. Paret, M. A. Ocsoy, S. Kunwar, T. Chen, M. You and W. Tan, *ACS Nano*, 2013, **7**, 8972.
15 K. R. Raghupathi, R. T. Koodali and A. C. Manna, *Langmuir*, 2011, **27**, 4020.
16 Y. Zhang, X. Gao, L. Zhi, X. Liu, W. Jiang, Y. Sun and J. Yang, *J. Inorg. Biochem.*, 2014, **130**, 74.
17 W. Lu, G. Liu, S. Gao, S. Xing and J. Wang, *Nanotechnology*, 2008, **19**, 445711.
18 Q. Deng, X. Duan, D. H. Ng, H. Tang, Y. Yang, M. Kong, Z. Wu, W. Cai and G. Wang, *ACS Appl. Mater. Interfaces*, 2012, **4**, 6030.
19 S. Jaiswal, P. McHale and B. Duffy, *Colloids Surf., B*, 2012, **94**, 170.
20 S. C. Motshekga, S. S. Ray, M. S. Onyango and M. N. Momba, *J. Hazard. Mater.*, 2013, **262**, 439.
21 T. Siva Vijayakumar, S. Karthikeyeni, S. Vasanth, A. Ganesh, G. Bupesh, R. Ramesh, M. Manimegalai and P. Subramanian, *J. Nanosci.*, 2013, 7.
22 T. Shoeib, K. M. Siu and A. C. Hopkinson, *J. Phys. Chem. A*, 2002, **106**, 6121.
23 Y. W. Heo, S. J. Pearton, D. P. Norton and F. Ren, *Semiconductor device-based sensors for gas, chemical, and biomedical applications*, CRC Press, 2011.
24 C. K. Thai, H. Dai, M. Sastry, M. Sarikaya, D. T. Schwartz and F. Baneyx, *Biotechnol. Bioeng.*, 2004, **87**, 129.
25 A. Legler, A. Kazachenko, V. Kazbanov, O. Per'yanova and O. Veselova, *Pharm. Chem. J.*, 2001, **35**, 501.
26 S. Agnihotri, S. Mukherji and S. Mukherji, *RSC Adv.*, 2014, **4**, 3974.
27 S. Mohanty, S. Mishra, P. Jena, B. Jacob, B. Sarkar and A. Sonawane, *Nanomed: Nanotechnol. Biol. Med.*, 2012, **8**, 916.
28 M. W. Forbes, M. F. Bush, N. C. Polfer, J. Oomens, R. C. Dunbar, E. R. Williams and R. A. Jockusch, *J. Phys. Chem. A*, 2007, **111**, 11759.

29 A. Aliaga, C. Garrido, P. Leyton, G. Diaz F., J. S. Gomez-Jeria, T. Aguayo, E. Clavijo, M. Campos-Vallette and S. Sanchez-Cortes, *Spectrochim. Acta, Part A*, 2010, **76**, 458.
30 C. Garrido, T. Aguayo, E. Clavijo, J. Gómez-Jeria and M. Campos-Vallette, *J. Raman Spectrosc.*, 2013, **44**, 1105.
31 S. K. Das, M. M. R. Khan, A. K. Guha and N. Naskar, *Green Chem.*, 2013, **15**, 2548.
32 W. Xie, Y. Li, W. Sun, J. Huang, H. Xie and X. Zhao, *J. Photochem. Photobiol., A*, 2010, **216**, 149.
33 S. Ghosh, V. Goudar, K. Padmalekha, S. Bhat, S. Indi and H. Vasan, *RSC Adv.*, 2012, **2**, 930.
34 S. A. Ansari, M. M. Khan, M. O. Ansari, J. Lee and M. H. Cho, *J. Phys. Chem. C*, 2013, **117**, 27023.
35 M. Schmidt, A. Masson and C. Brechignac, *Phys. Rev. Lett.*, 2003, **91**, 243401.
36 G. A. Sotiriou, A. Meyer, J. T. Knijnenburg, S. Panke and S. E. Pratsinis, *Langmuir*, 2012, **28**, 15929.
37 P. Prieto, V. Nistor, K. Nouneh, M. Oyama, M. Abd-Lefdil and R. Díaz, *Appl. Surf. Sci.*, 2012, **258**, 8807.
38 Y. Chi, L. Zhao, Q. Yuan, X. Yan, Y. Li, N. Li and X. Li, *J. Mater. Chem.*, 2012, **22**, 13571.
39 S. Song, B. You, Y. Zhu, Y. Lin, Y. Wu and X. Ge, *Cryst. Growth Des.*, 2014, **14**, 38.
40 V. Datsyuk, M. Kalyva, K. Papagelis, J. Parthenios, D. Tasis, A. Siokou, I. Kallitsis and C. Galiotis, *Carbon*, 2008, **46**, 833.
41 H. J. Kim, I.-S. Bae, S.-J. Cho, J.-H. Boo, B.-C. Lee, J. Heo, I. Chung and B. Hong, *Nanoscale Res. Lett.*, 2012, **7**, 1.
42 B. Xia, S. J. Xiao, D. J. Guo, J. Wang, J. Chao, H. B. Liu, J. Pei, Y. Q. Chen, Y. C. Tang and J. N. Liu, *J. Mater. Chem.*, 2006, **16**, 570.
43 A. D. Fuchs and J. C. Tiller, *Angew. Chem., Int. Ed.*, 2006, **45**, 6759.
44 F. Cheng, J. W. Betts, S. M. Kelly, J. Schaller and T. Heinze, *Green Chem.*, 2013, **15**, 989.
45 J. P. Ruparelia, A. K. Chatterjee, S. P. Duttagupta and S. Mukherji, *Acta Biomater.*, 2008, **4**, 707.
46 M. Auffan, J. Rose, J. Y. Bottero, G. V. Lowry, J. P. Jolivet and M. R. Wiesner, *Nat. Nanotechnol.*, 2009, **4**, 634.
47 J. R. Morones, J. L. Elechiguerra, A. Camacho, K. Holt, J. B. Kouri, J. T. Ramírez and M. J. Yacaman, *Nanotechnology*, 2005, **16**, 2346.
48 S. C. Hayden, G. Zhao, K. Saha, R. L. Phillips, X. Li, O. R. Miranda, V. M. Rotello, M. A. El-Sayed, I. Schmidt-Krey and U. H. Bunz, *J. Am. Chem. Soc.*, 2012, **134**, 6920.
49 I. Sondi and B. Salopek-Sondi, *J. Colloid Interface Sci.*, 2004, **275**, 177.
50 O. Bondarenko, K. Juganson, A. Ivask, K. Kasemets, M. Mortimer and A. Kahru, *Arch. Toxicol.*, 2013, **87**, 1181.
51 A. Agarwal, T. L. Weis, M. J. Schurr, N. G. Faith, C. J. Czuprynski, J. F. McAnulty, C. J. Murphy and N. L. Abbott, *Biomaterials*, 2010, **31**, 680.
52 C. Y. Chu, F. C. Peng, Y. F. Chiu, H. C. Lee, C. W. Chen, J. C. Wei and J. J. Lin, *PLoS One*, 2012, **7**, e38360.
53 Z. Shi, K. Neoh, S. Zhong, L. Yung, E. Kang and W. Wang, *J. Biomed. Mater. Res., Part A*, 2006, **76**, 826.
54 M. Stevanović, I. Bračko, M. Milenković, N. Filipović, J. Nunić, M. Filipič and D. P. Uskoković, *Acta Biomater.*, 2014, **10**, 151.
55 V. Mersch-Sundermann, S. Knasmüller, X.-J. Wu, F. Darroudi and F. Kassie, *Toxicology*, 2004, **198**, 329.
56 C. Carlson, S. Hussain, A. Schrand, L. K. Braydich-Stolle, K. Hess, R. Jones and J. Schlager, *J. Phys. Chem. B*, 2008, **112**, 13608.
57 M. J. Piao, K. A. Kang, I. K. Lee, H. S. Kim, S. Kim, J. Y. Choi, J. Choi and J. W. Hyun, *Toxicol. Lett.*, 2011, **201**, 92.
58 A. Nel, T. Xia, L. Mädler and N. Li, *Science*, 2006, **311**, 622.
59 J. Fabrega, S. R. Fawcett, J. C. Renshaw and J. R. Lead, *Environ. Sci. Technol.*, 2009, **43**, 7285.
60 E. Navarro, F. Piccapietra, B. Wagner, F. Marconi, R. Kaegi, N. Odzak, L. Sigg and R. Behra, *Environ. Sci. Technol.*, 2008, **42**, 8959.
61 Z. M. Xiu, Q. B. Zhang, H. L. Puppala, V. L. Colvin and P. J. J. Alvarez, *Nano Lett.*, 2012, **12**, 4271.
62 X. Yang, A. P. Gondikas, S. M. Marinakos, M. Auffan, J. Liu, H. Hsu-Kim and J. N. Meyer, *Environ. Sci. Technol.*, 2011, **46**, 1119.
63 A. Lass, A. Suessenbacher, G. Wolkart, B. Mayer and F. Brunner, *Mol. Pharmacol.*, 2002, **61**, 1081.
64 P. Tripathi, T. P. Singh, M. Chandra and M. K. Misra, *Int. J. Biol. Med. Res.*, 2010, **1**, 15.